Mediator complex subunit 16 is down-regulated in papillary thyroid cancer, leading to increased transforming growth factor-β signaling and radioiodine resistance

Received for publication, December 21, 2019, and in revised form, June 10, 2020 Published, Papers in Press, June 12, 2020, DOI 10.1074/jbc.RA119.012404

Hongwei Gao[1,2,‡], Peirong Bai[1,2,‡], Lin Xiao[1], Mengjia Shen[1,3], Qiuxiao Yu[4], Yuanyuan Lei[4], Wenting Huang[5], Xiang Lin[1], Xinyi Zheng[1], Tao Wei[6], Yong Jiang[3], Feng Ye[1,2,*], and Hong Bu[1,2,3,*]

From the [1]Laboratory of Pathology, West China Hospital, Sichuan University, Chengdu, China, the [2]Key Laboratory of Transplant Engineering and Immunology, Ministry of Health, West China Hospital, Sichuan University, Chengdu, China, the [3]Department of Pathology, West China Hospital, Sichuan University, Chengdu, China, the [4]National Cancer Center/National Clinical Research Center for Cancer/Cancer Hospital & Shenzhen Hospital, Chinese Academy of Medical Science and Peking Union Medical College, Shenzhen, China, the [5]National Cancer Center/National Clinical Research Center for Cancer/Cancer Hospital, Chinese Academy of Medical Science and Peking Union Medical College, Beijing, China, and the [6]Department of Thyroid Surgery, West China Hospital, Chengdu, Sichuan University, Chengdu, China

Edited by Qi-Qun Tang

Mediator complex subunit 16 (MED16) is a component of the mediator complex and functions as a coactivator in transcriptional events at almost all RNA polymerase II–dependent genes. In this study, we report that the expression of MED16 is markedly decreased in papillary thyroid cancer (PTC) tumors compared with normal thyroid tissues. *In vitro*, MED16 overexpression in PTC cells significantly inhibited cell migration, enhanced sodium/iodide symporter expression and iodine uptake, and decreased resistance to radioactive ^{131}I (RAI). Conversely, PTC cells in which MED16 had been further knocked down (MED16^{KD}) exhibited enhanced cell migration, epithelial–mesenchymal transition, and RAI resistance, accompanied by decreased sodium/iodide symporter levels. Moreover, cell signaling through transforming growth factor β (TGF-β) was highly activated after the MED16 knockdown. Similar results were obtained in MED12^{KD} PTC cells, and a co-immunoprecipitation experiment verified interactions between MED16 and MED12 and between MED16 and TGF-βR2. Of note, the application of LY2157299, a potent inhibitor of TGF-β signaling, significantly attenuated MED16^{KD}-induced RAI resistance both *in vitro* and *in vivo*. In conclusion, our findings indicate that MED16 reduction in PTC contributes to tumor progression and RAI resistance via the activation of the TGF-β pathway.

Thyroid cancer has been the most prevalent endocrine malignancy over the past few years, with the fastest growing incidence globally (1), among which papillary thyroid cancer (PTC) is the most common histologic type and accounts for ~80% of all cases (2). The increased incidence of PTC can be attributed to genetic mutations, iodine intake changes, radiation exposure, and so on (3). In the clinic, radioactive iodine (RAI) therapy is conventionally required after surgery to prevent disease recurrence and eliminate minor and residual lesions (4). Most PTC patients benefit from RAI; however, 6–20% of patients still relapse with distant metastases, and 65% of this population develops radioiodine refractory disease accompanied by dedifferentiated tumors, which have higher degrees of malignancy and worse outcomes (5, 6). Therefore, there is an urgent need to elucidate the mechanisms underlying ^{131}I resistance and to improve the therapeutic outcome of PTC patients with RAI-refractory disease.

Previous studies have reported several pathways involved in papillary thyroid cancer, among which the overactivation of phosphatidylinositol 3-kinase/AKT and/or MAPK/ERK signaling is required for PTC tumorigenesis and progression. According to a genomic analysis of PTC, more than 70% of patients have MAPK overactivation because of BRAF and RAS mutations (7). The TGF-β pathway, which is closely related to these two pathways, has also been investigated in PTC. Interestingly, TGF-β signaling seems to have a double-edged effect on tumor progression. Activation of the TGF-β pathway can slow down cell proliferation, arrest the cell cycle (7, 8), and facilitate apoptosis (9). Other studies have demonstrated that the activation of the TGF-β pathway can promote EMT during tumorigenesis and hence lead to local invasion and distant metastasis (10). Over recent decades, the regulatory effect of TGF-β signaling on NIS expression has drawn attention because of its critical participation in iodine uptake, which potentially affects RAI treatment efficacy in patients with thyroid cancer. In PTC, accumulating studies have shown that TGF-β signaling is significantly activated in the invasive region of the tumor and negatively regulates NIS expression, which closely correlates with radiotherapy sensitivity in PTC (11, 12). Thus, the activation of TGF-β may result in the decreased iodine uptake ability of tumor cells and finally lead to the therapeutic tolerance of radioactive iodine.

MED16 is a subunit of the mediator complex, a multimeric protein complex serving as a bridge in conveying information from specific transcription factors to RNA polymerase II. Growing evidence has indicated that mediator complex subunits exhibit cancer-specific transcription profiles, suggesting the implication of different subunits in carcinogenesis and

This article contains supporting information.
‡These authors contributed equally to this work.
*For correspondence: Feng Ye, fengye@scu.edu.cn; Hong Bu, hongbu@scu.edu.cn.

development (13, 14). To date, studies of MED1, MED12, MED28, CDK8, and cyclins have been well-established, and related disease subtypes display either mutated or changed expression of these molecules (14). A published study showed that in colon and lung cancer cells, cytoplasmic MED12 negatively regulates TGF-βR2 by physical interaction and therefore suppresses TGF-β signal transduction, whereas TGF-β is highly activated after MED12 loss, leading to an EMT-like phenotype and drug resistance (15). The expression pattern of MED16, an important subunit of this mediator family, is rarely reported in PTC, so its expression pattern and regulatory role need to be elucidated.

In our study, we found that the expression of MED16 was significantly reduced in tumors compared with adjacent normal tissue, indicating a potential anti-oncogenetic property of MED16 in PTC carcinogenesis. In papillary thyroid cancer cells, MED16 overexpression significantly inhibited cell migration, enhanced NIS expression and iodine uptake, and facilitated PTC radioactive iodine treatment. However, shRNA-mediated MED16 depletion significantly facilitated cell migration, reduced NIS expression and ^{131}I uptake, and promoted radioactive iodine treatment failure. All of these effects are mediated by activation of TGF-β signaling, and the blockade of this pathway using a specific TGF-β inhibitor successfully rescued radioiodine resistance both *in vivo* and *in vitro*. Not surprisingly, similar results were observed in MED12-knockdown PTC cells, and the co-IP data implied physical interactions between MED16/MED12 and MED16/TGF-βR2, suggesting that MED16 and MED12 cooperate to act as suppressors of TGF-β pathway activation by binding to TGF-βR2. Taken together, this study suggests that MED16^{KD}-mediated TGF-β activation contributes to malignant cell transformation and radioiodine resistance in PTC, enhancing the development of new combination therapies for PTC patients with RAI resistance.

Results

Low expression of MED16 in PTC samples

We evaluated MED16 expression profiles and clinical relevance in thyroid cancer using the Genotype-Tissue Expression (GTEx), The Cancer Genome Atlas (TCGA), and the THCA data sets. Of significance, MED16 was underexpressed in PTC samples compared with normal tissues (Fig. 1*A*). Genetic drivers have distinct signaling consequences; thus, PTC samples were categorized into *Braf*-like and Ras-like subtypes based on unique gene signatures (16). As shown in Fig. 1*B*, MED16 expression did not differ between Braf-like and Ras-like PTCs across the THCA series. However, there was an increase in MED16 expression in Braf-mutant PTC *versus* non-Braf mutant tumors (Fig. 1*C*). In addition, the frequency of *Braf* alterations was lower in PTC with low MED16 expression compared with PTC with high MED16 expression (Fig. 1*D*). To determine whether these results were clinically pertinent, we examined the expression level of MED16 in 12 paired PTC clinical samples using qPCR. A negative correlation was found between the MED16 expression level and the degree of tissue malignancy (Fig. 1*E*). These results suggested that MED16 might play an anti-oncogenetic role in the development of thyroid tumors.

Med16 was involved in cell migration and EMT in PTC cells

To investigate the functional role of MED16 in PTC, we constructed stable MED16 overexpression and knockdown PTC cell lines by infecting cells with lentivirus harboring the MED16 CDS region or shMED16 and validated the results at the mRNA and protein levels. The qRT-PCR results showed that the knockdown efficiency of shRNA1 and shRNA2 reached ~80 and 60% in both PTC cell lines, respectively, and the overexpression vector led to a 136-fold increase in MED16 expression compared with that of the control vector in B-CPAP cells; MED16 expression increased 49-fold in TPC-1 cells (Fig. 2, *C* and *D*). Similarly, the protein level of MED16 was validated by Western blotting (Fig. 2, *A* and *B*). In subsequent experiments, shRNA1 was chosen because of its high knockdown efficiency. To study the role of MED16 in PTC cell migration, wound-healing analysis was conducted, showing that MED16^{KD} significantly increased the migration rates of TPC-1 and B-CPAP cells and that MED16^{OE} inhibited the migration of PTC cells. (Fig. 2, *E–H*). Consistently, Transwell assays confirmed that MED16 suppressed the migration ability of PTC cells (Fig. S1). For cell morphology, the spindle length of MED16^{KD} B-CPAP cells was found to be significantly longer than that of pLKO.1 vector-infected cells, and MED16^{OE} cells were significantly more closely connected and grew in a colony-like manner (Fig. 3*A*), but no significant morphological changes were observed in TPC-1 cells (data not shown). Considering the change in motor ability, we proposed that MED16 could be involved in EMT in PTC cells. To validate this hypothesis, we used Western blotting and qPCR to detect both epithelial markers (E-cadherin) and mesenchymal markers (N-cadherin and vimentin). As shown in Fig. 3 (*D* and *E*), the suppression of MED16 occurred in parallel with the down-regulation of E-cadherin and the up-regulation of vimentin in both PTC cell lines. The overexpression of MED16 showed the opposite effect, and similar results were found by qPCR (Fig. 3, *B* and *C*). The mRNA levels of EMT-related transcription factors (Snail, Slug, and Twist) (Fig. S2) and MMP families (MMP1, MMP2, MMP9, and MMP13) were also assessed in MED16^{KD} cells and vector cells (Fig. 3, *F* and *G*), implying that the suppression of MED16 resulted in elevated transcriptional activity of these migration-related genes. These data indicate that MED16 knockdown promoted cell motility and facilitated EMT in PTC cells.

Med16 affected radioiodine response by regulating NIS in PTC cells

To determine the involvement of MED16 in radioiodine resistance in PTC, two cell lines were incubated with ^{131}I for 48 h, and the cytotoxicity was analyzed by CCK-8 assay (Fig. 4*A*). The cell viability of the MED16^{KD} groups was significantly higher than that of the control cells, indicating a higher tolerance to ^{131}I, and the MED16^{OE} groups were more sensitive to ^{131}I (Fig. 4*B*). Subsequently, the I^- uptake ability was measured in both TPC-1 and B-CPAP cells. Compared with the control group, the iodine uptake capacity decreased to 73 and 74.5% in

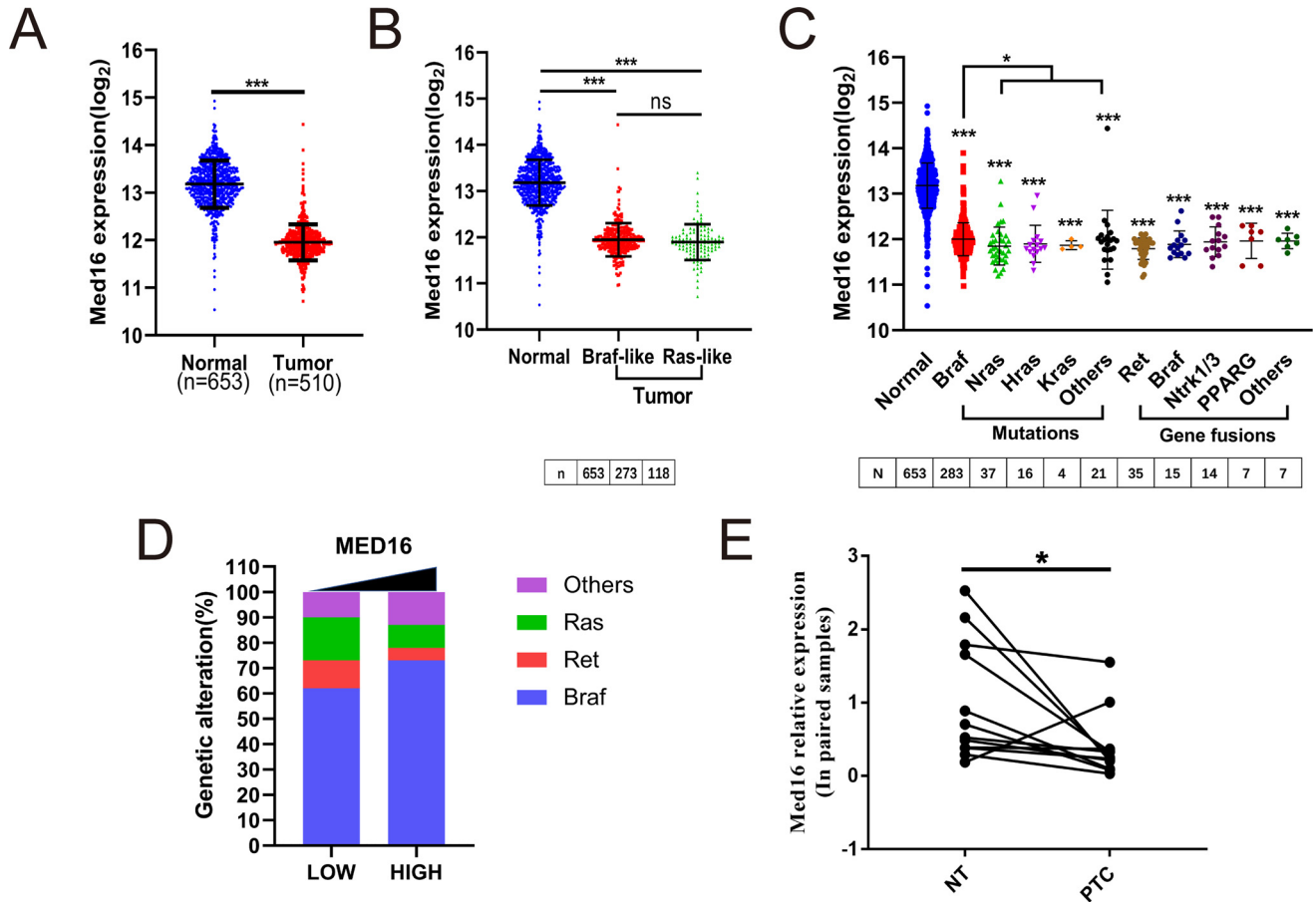

Figure 1. Low expression of MED16 in PTC compared with in normal thyroid. *A*, MED16 expression in normal thyroid in the GTEx data set ($n = 653$) and PTC ($n = 510$) in the THCA TCGA data set. *B*, MED16 expression in PTC with Braf-like ($n = 273$) and Ras-like (118) genetic signatures. *C*, MED16 expression in PTC with indicated genetic alterations. *D*, frequency (%) of indicated genetic alterations in PTC with low (<11.92) *versus* high (>11.92) MED16 expression. *E*, expression level of MED16 was significantly underexpressed in tumor tissue, when compared with paired normal thyroid (*NT*) tissue. *ns*, not significant. *, $P < 0.05$; **, $P < 0.01$; ***, $P < 0.001$.

MED16^{KD} TPC-1 cells and decreased to 76.6 and 81.5% in MED16^{KD} B-CPAP cells, and the iodine uptake capacity increased in MED16^{OE} PTC cells (Fig. 4*C*). To determine the possible cause of ^{131}I resistance, NIS expression in control and MED16^{KD} cells was detected by Western blotting. Significant reductions in NIS at the protein level were observed after MED16 knockdown in both PTC cell lines (Fig. 4, *D* and *E*). To test this further, TPC-1 and B-CPAP cell lines were transfected with a *p*NIS-Luc reporter plasmid containing the −2926/−1 core promoter and the −9298/−9244 NIS upstream enhancer. NIS promoter activity was induced in both MED16-overexpressing PTC cell lines. These data implied that MED16 loss decreased radioiodine sensitivity by reducing the I^- uptake capacity, which was mediated by NIS suppression in PTC cells.

Med16^{kd} activated the TGF-β pathway in PTC cells

To unravel the mechanism underlying MED16^{KD}-mediated EMT and ^{131}I resistance, the activation of the TGF-β pathway was investigated. In both B-CPAP and TPC-1 cells, MED16 knockdown significantly increased the phosphorylation level of Smad2 and Erk1/2, as well as the expression of TGF-βR2, whereas MED16 overexpression inhibited TGF-β pathway activity (Fig. 5, *A–D*). Furthermore, marked elevation of TGF-β target genes (ANGPTL4, TAGLN, CRY6,1 and CTGF) was detected by qPCR in both MED16^{KD} PTC cell lines (Fig. 5*E*), and a predominant translocation of Smad2 from the cytoplasm to the nucleus was observed in MED16^{KD} cells; however, the expression of Smad2 in the nucleus was decreased in both MED16^{OE} cell lines compared with control cell lines (Fig. 5, *F* and *G*). The mRNA levels of ALK5 and TGF-β family signals (*e.g.* activin and BMPs) were assessed; however, we did not detect the up-regulation of ALK5 activin and BMPs except the TGF-β target genes (Fig. 5*E*). We speculated that the activation of the TGF-β pathway was due to the increased ligand reactivity caused by the up-regulation of TGF-βR2. To test this hypothesis, SMAD activity was studied by a luciferase reporter system in MED16 knockdown cells transfected with the pGMSMAD-Lu plasmid, and SMAD activity was significantly increased in MED16^{KD} cells compared with the control cells (Fig. S2). These data indicated potent TGF-β activation induced in PTC cells with MED16^{KD}.

Med12^{kd} promoted PTC cell migration, ^{131}I resistance, and TGF-β activation

MED12 is another subtype of the mediator complex that was reported to inhibit the TGF-β pathway by binding to TGF-βR2

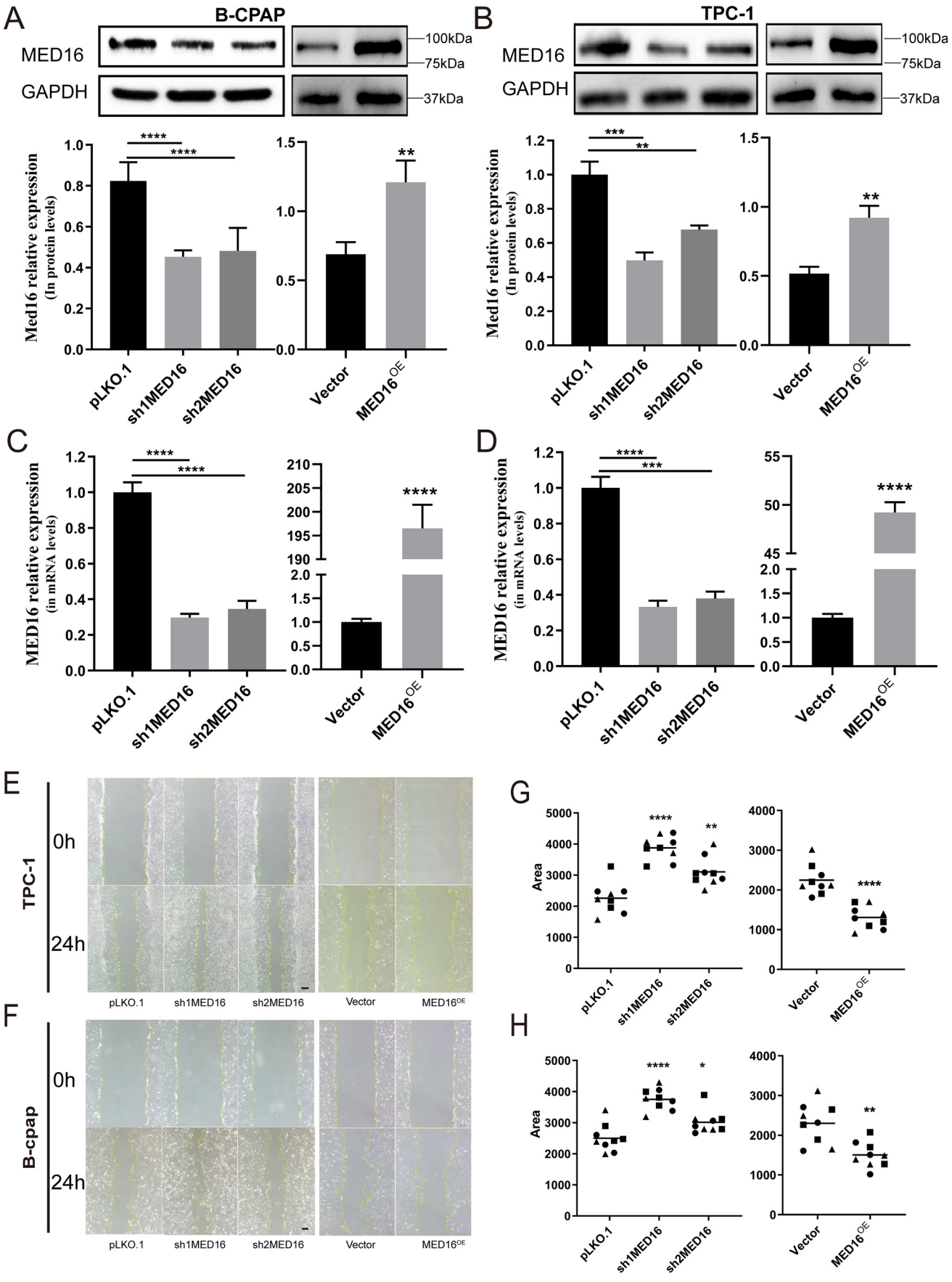
A
B-CPAP
MED16
GAPDH
100kDa
75kDa
37kDa
Med16 relative expression
(In protein levels)
pLKO.1
sh1MED16
sh2MED16
Vector
MED16OE
B
TPC-1
C
MED16 relative expression
(in mRNA levels)
D
E
TPC-1
0h
24h
F
B-cpap
G
Area
H

in the cytoplasm of various tumor cells (15). To clarify the role of MED12 in thyroid cancer, stable B-CPAP and TPC-1 strains with MED12 knockdown were constructed as well. The knockdown efficiency of shRNA1 and shRNA2 reached 86 and 22%, respectively (data not shown). The Transwell experiment showed that MED12^{KD} reproduced the phenotypes induced by MED16^{KD} and that the cell migration ability was significantly enhanced (Fig. S3). MED12 depletion also led to RAI therapy resistance, which was positively correlated with knockdown efficacy (Fig. 6*A*). In addition, we discovered that the protein levels of p-Smad2, p-Erk1/2, and TGF-βR2 in MED12^{KD} cells were remarkably increased, indicating high activation of TGF-β signaling after MED12 knockdown (Fig. 6*B*). To further explore the relationship between MED12 and MED16, we analyzed the tolerance of MED12 and MED16 double-knockdown cells to radioactive iodine. However, compared with MED12^{KD} or MED16^{KD} cells, cell viability was improved in cells with knockdown of both MED16 and MED12, and the expression of NIS was also decreased (Fig. 6, *C–E*). Therefore, we believe that there is a synergistic effect between MED16 and MED12. To investigate the mechanism underlying MED16-mediated TGF-β activation, the subcellular localization of MED16 was first assessed by immunofluorescence. As shown in Fig. 6*H*, MED16 was abundantly expressed in the cytoplasm. In addition, the co-IP experiment showed that MED16 coprecipitated with MED12 and TGF-βR2 in PTC cells (Fig. 6*F*), which suggested that MED16 might physically interact with MED12 and therefore synergistically inhibit the activation of TGF-β by binding to its receptor TGF-βR2. However, MED12 and TGF-βR2 interact in the cytoplasm, so to further clarify the interrelationship between MED12/MED16/TGF-βR2, pLKO.1 and MED12^{KD} TPC-1 cell cytoplasmic fractions were used for co-IP experiments. The results showed that the level of TGF-βR2 was significantly increased in MED12^{KD} cells, but MED12 knockdown did not affect the interaction of MED16 with TGF-βR2 (Fig. 6*G*). Therefore, MED16 may mediate the interaction of MED12 and TGF-βR2 to play a key role in the regulation of the TGF-β pathway.

TGF-β inhibitor rescued the radioiodine resistance induced by MED16 and MED12 knockdown in PTC cells

Considering the critical involvement of the TGF-β pathway in the drug resistance of many tumors, we proposed that the ^{131}I resistance induced by MED16 and MED12 knockdown was also mediated by TGF-β signaling. To verify our hypothesis, LY2157299, a specific inhibitor of TGF-β, was applied to block this pathway. As shown in Fig. 7*A*, the phosphorylation level of Smad2 in B-CPAP cells was reduced by LY2157299 (5–20 μM) in a dose-dependent manner after a 48-h incubation, and 5 μM was chosen as the optimal dosage with statistical significance in the following experiments. The control, MED16^{KD}, and MED12^{KD} PTC cells were treated with ^{131}I in the presence or absence of LY2157299 at 5 μM. As shown in Fig. 7*B*, the dampened response to ^{131}I treatment in MED16^{KD} or MED12^{KD} cells was dramatically rescued by LY2157299 in both B-CPAP and TPC-1 cells. To determine the reason that the TGF-β inhibitor attenuated radioiodine resistance, I^- uptake in MED12^{KD} and MED16^{KD} cells was assessed. A significant increase in I^- uptake was observed after incubation with LY2157299 in both PTC cell lines (Fig. 7*C*).

Tgf-β inhibitor attenuated MED16^{KD}-induced radioiodine resistance in PTC in vivo

To investigate MED16 function *in vivo*, we conducted a subcutaneous tumorigenesis experiment in nude mice, as shown in Fig. 8*A*, When compared with pLKO.1 tumors treated with ^{131}I, the growth of MED16^{KD} tumors with the same treatment was remarkably faster (Fig. 8*B*). Interestingly, no difference was detected in the size of pLKO.1 tumors and MED16^{KD} tumors obtained from mice without any treatment, as shown in Fig. 8 (*G* and *I*). These results demonstrated that MED16 depletion facilitated radioiodine resistance instead of enhancing tumor growth *in vivo*. Most importantly, the tumor size of MED16^{KD} tumor-bearing mice treated with both LY2157299 and ^{131}I was dramatically decreased compared with the MED16^{KD} tumor-bearing mice that received ^{131}I alone, indicating that LY2157299 significantly improved the therapeutic effect of ^{131}I *in vivo*, which is consistent with the results of the cell experiments. In addition, MED16^{KD} tumors treated with LY2157299 + ^{131}I also showed increased ^{131}I sensitivity compared with that in pLKO.1 tumors treated with ^{131}I therapy, indicating that in addition to activation of TGF-β signaling induced by MED16 knockdown, endogenous TGF-β signaling was also suppressed by LY2157299 in MED16^{KD} tumors (Fig. 8, *B–D*). We evaluated the possible association between MED16 level and patient outcome with or without RAI therapy of THCA data sets. Overall, no significant difference in survival rate was detected between PTC patients with high and low tumoral MED16 expression among the entire cohort (n = 481) (p = 0.5409) (Fig. 8*E*). However, in the subgroup of PTC patients who received RAI therapy (n = 146), the disease-free survival rate was positively correlated with the expression level of tumoral MED16 in patients, although the difference was not statistically significant (p = 0.0896) (Fig. 8*F*). Importantly, there were no significant differences in clinical staging attributes for RAI or non–RAI treatment groups stratified by MED16 tumoral expression (Tables S1 and S2). Similarly, the proposed mechanism underlying MED16^{KD}-induced ^{131}I resistance was validated *in vivo* by detecting the expression of several key proteins, including p-smad2/smad2, TGF-βR2, and NIS. The Western blotting data illustrated elevated TGF-

Figure 2. MED16 was involved in human PTC cell migration *in vitro*. *A* and *B*, knockdown or overexpression efficiency in protein level were analyzed. GAPDH was used as an endogenous control. Western blotting analyses were performed, and proteins were detected with an antibody against MED16. *C* and *D*, knockdown or overexpression efficiency in mRNA level were analyzed. GAPDH was used as an endogenous control. *E* and *F*, the wound-healing assay was used to assess the biological function of MED16 on cell migration of B-CPAP and TPC-1 cells after treatment, *Scale bar*, 20 μm. Wound closure was analyzed by ImageJ. Each symbol (*circle*, *triangle*, and *square*) represents different batches separately. *G* and *H*, percentages of wound closures in the wound-healing assays. *, $P < 0.05$; **, $P < 0.01$; ***, $P < 0.001$; ****, $P < 0.0001$.

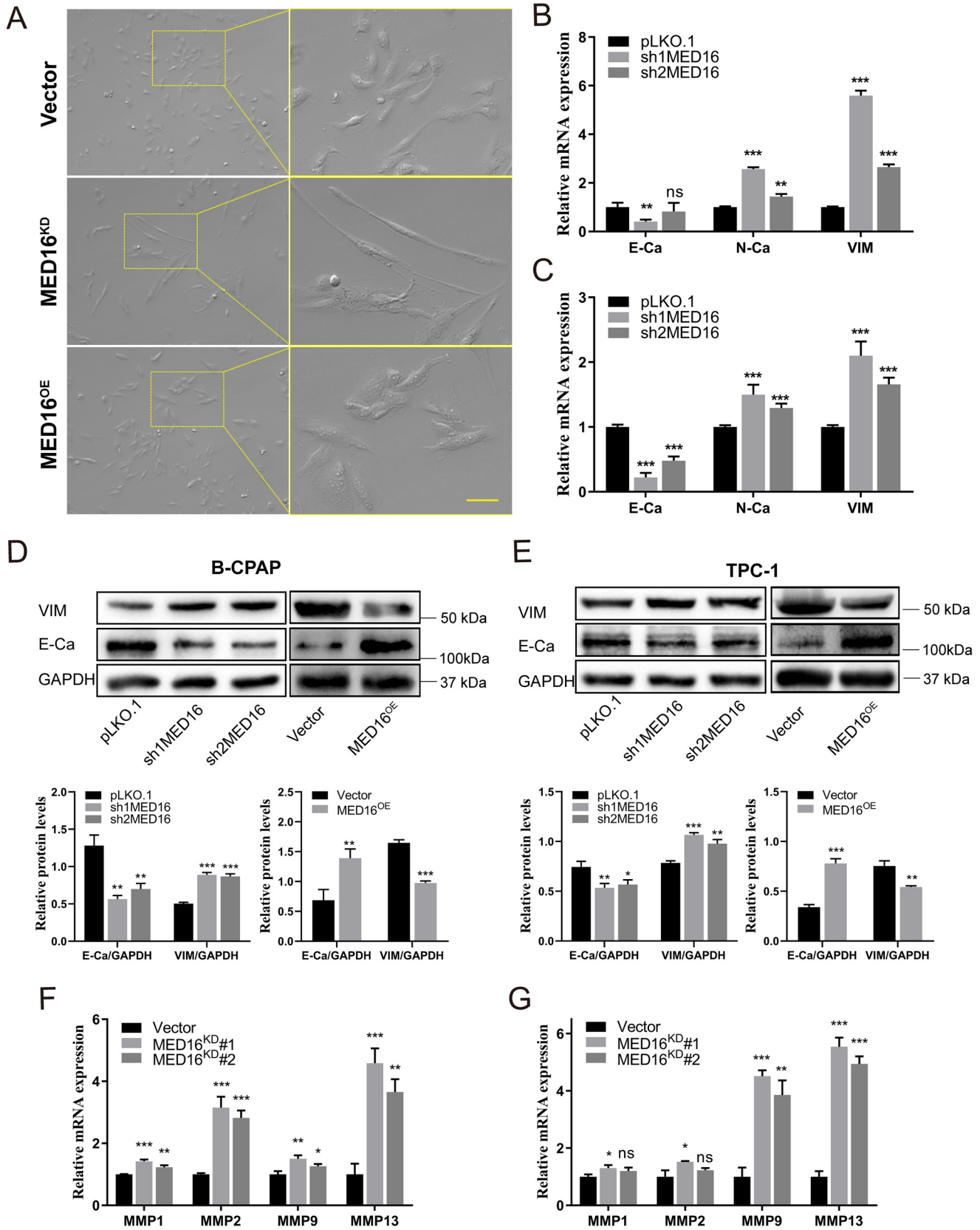

Figure 3. Knockdown of MED16 promotes EMT changes in human PTC cells. *A*, cell morphology changed in MED16^{KD} and MED16^{OE} B-CPAP. The spindle length of MED16^{KD} cells was significantly longer than that of pLKO.1 cells; MED16^{OE} cells grew in a colony-like manner. *Scale bar*, 50 μm. *B–E*, MED16^{KD} leads to induction of EMT marker genes and a panel of migration-related genes. mRNA and protein expression analysis by qRT-PCR and Western blotting of migration-related genes MMP1, MMP2, MMP9, and MMP13 and EMT marker genes vimentin and E-cadherin in B-CPAP (*B*, *D*, and *F*) and TPC-1 (*C*, *E*, and *G*) cells expressing pLKO.1 controls or shRNAs targeting MED16 is shown. *, $P < 0.05$; **, $P < 0.01$; ***, $P < 0.001$; ****, $P < 0.0001$.

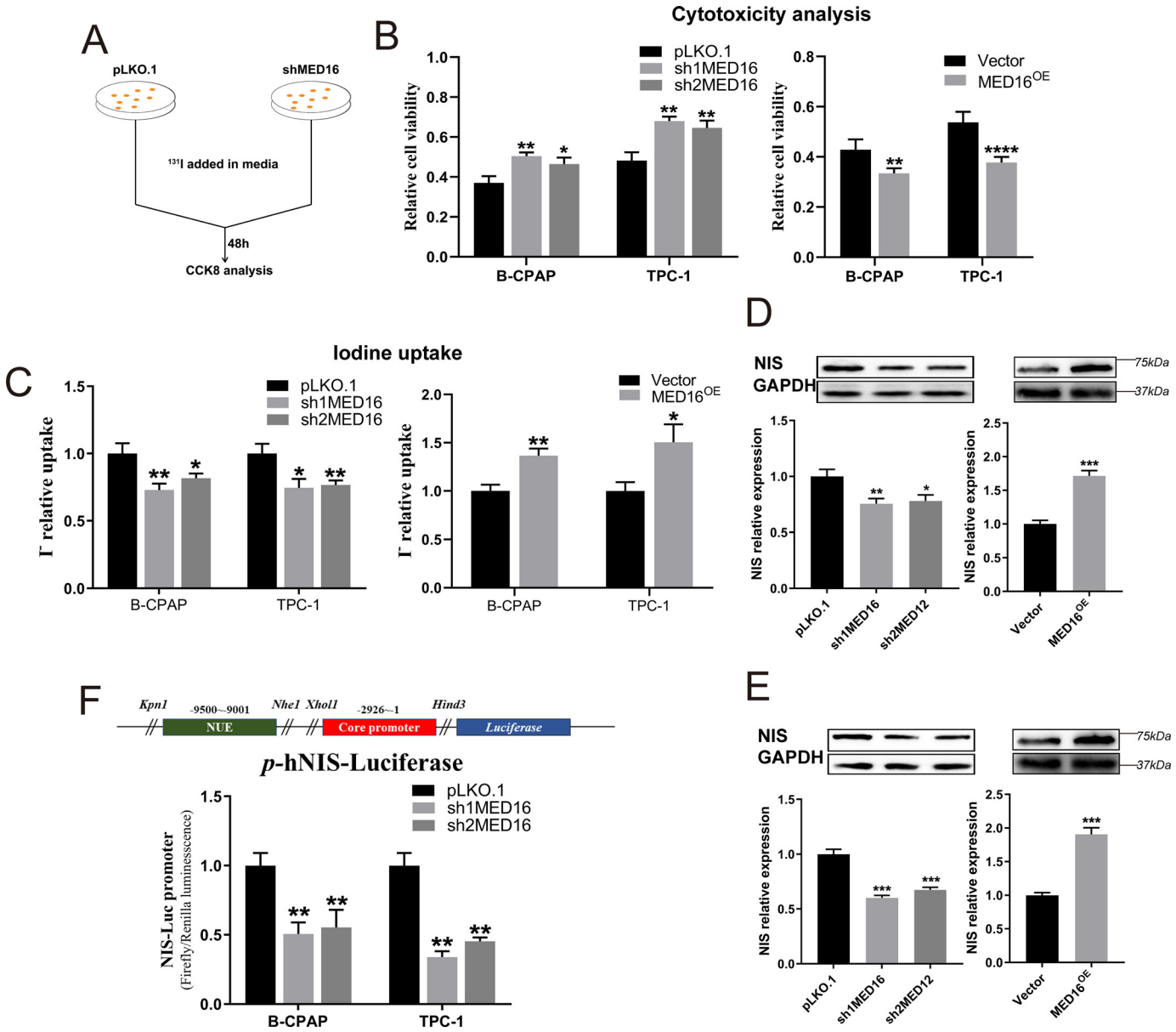

Figure 4. MED16^{KD} induced radioiodine resistance by down-regulating NIS in PTC cells. *A* and *B*, RAI cytotoxicity in TPC-1 and B-CPAP cells was analyzed by CCK8. *C*, RAI uptake analysis of TPC-1 and B-CPAP cells with different MED16 expression. *D* and *E*, MED16^{KD} results in strong reduction of NIS protein level, and MED16^{OE} induces the expression of NIS. Western blotting analysis of B-CPAP (*D*) and TPC-1 (*E*) cells is shown. GAPDH was used as a loading control. Densitometric quantification of NIS levels normalized to GAPDH levels and presented as fold change compared with Vector-control cells. *F*, luciferase reporter assays showed MED16^{KD} inhibited the expression of NIS. *NS*, not significant. *, $P < 0.05$; **, $P < 0.01$; ***, $P < 0.001$.

βR2 and p-Smad2 levels, as well as decreased expression of NIS in MED16^{KD} tumors compared with pLKO.1 tumors (Fig. 8, *H* and *I*). These data indicate that the activation of the TGF-β pathway induced by MED16 knockdown was critical for tumor survival even after ^{131}I treatment, suggesting that combination therapy with RAI and TGF-β inhibitor might be a favorable approach for treating PTC patients with MED16 mutations.

Discussion

Thyroid cancer has been rated as the most frequent endocrine malignancy worldwide, and the number of newly diagnosed cases in China exceeded 190,000 in 2018 (17). Papillary thyroid cancer is characterized as a major subtype of differentiated thyroid cancer with a relatively favorable prognosis after surgery and conventional radioactive iodine therapy, which is a mainstay of PTC treatment. However, some PTC patients unfortunately develop local recurrence and distant metastasis because their thyroid tumor cells no longer take up iodine and hence are resistant to RAI treatment. The outcome of patients with RAI-refractory PTC is poor, and the 5-year disease-free survival rate is only 60–70% (18). Given this, exploring the relevant factors influencing RAI therapy efficacy and resensitizing RAI-refractory tumors to ^{131}I would tremendously improve the treatment and survival rate of PTC patients.

In thyroid cells, iodine uptake and accumulation are predominantly facilitated by NIS, which is expressed at the highest level in the thyroid compared with other organs (19). PTC cells

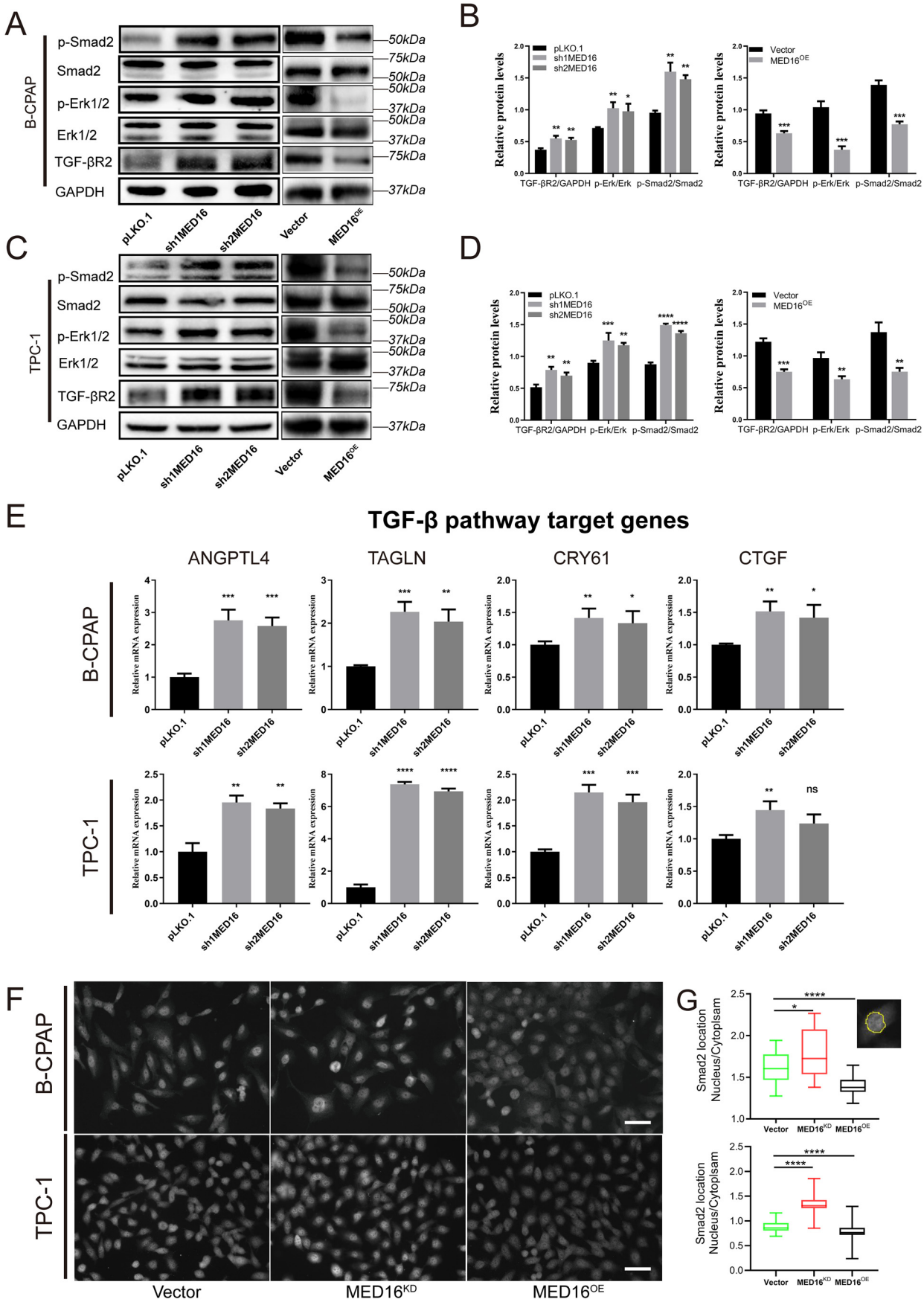
A
B-CPAP
p-Smad2
Smad2
p-Erk1/2
Erk1/2
TGF-βR2
GAPDH
50kDa
75kDa
50kDa
50kDa
37kDa
50kDa
37kDa
75kDa
37kDa
pLKO.1
sh1MED16
sh2MED16
Vector
MED16OE
B
pLKO.1
sh1MED16
sh2MED16
Relative protein levels
TGF-βR2/GAPDH
p-Erk/Erk
p-Smad2/Smad2
Vector
MED16OE
C
TPC-1
D
E
TGF-β pathway target genes
ANGPTL4
TAGLN
CRY61
CTGF
Relative mRNA expression
ns
F
Vector
MED16KD
MED16OE
G
Smad2 location
Nucleus/Cytoplsam

normally retain similar NIS expression and localization to follicular cells, allowing RAI to enter tumor cells to prevent local recurrence and distant metastasis. Therefore, impairment of NIS function is considered a hallmark of RAI resistance in a subset of PTC patients (20). In this study, we discovered that MED16 was a positive regulator of NIS expression in both PTC cells and tumor tissues, explaining the decreased sensitivity to ^{131}I treatment after MED16 knockdown. Likewise, we found that disease-free survival was positively correlated with MED16 levels in patients who received RAI treatment, also hinting at the relevance between MED16 expression and RAI resistance in the PTC group. Hence, MED16 might be identified as a feasible candidate biomarker of RAI response in PTC patients.

NIS expression can be down-regulated by the MAPK/ERK pathway, which affects its function. As a key molecule in MAPK signaling, the BRAF^{V600E} mutation is regarded as an exclusive oncogene that frequently occurs in PTC patients and is critical for tumor initiation and progression. Emerging results have unraveled a close association between the BRAF^{V600E} mutation and failure of RAI therapy in PTC (21, 22). As reported by Riesco-Eizaguirre *et al.* (11) and Costamagna *et al.* (23), the BRAF^{V600E} mutation enhanced TGF-β secretion, which stimulated the activation of SMAD and subsequently reduced NIS expression. Most importantly, this process was independent of MAPK signaling, which emphasizes the potential of a TGF-β inhibitor as a candidate therapeutic approach for regaining NIS function in PTC patients. As detected in our study, MED16 loss in PTC cell lines induced marked activation of TGF-β signaling represented by increased phosphorylation of Smad2 and ERK1/2, nuclear translocation of Smad2, up-regulation of TGF-βR2, and elevation of TGF-β target gene transcription. Moreover, the activation of TGF-β was detected in MED16^{KD} tumors in mice. These results are in accordance with the NIS reduction induced by MED16^{KD}, suggesting that MED16 can affect radioiodine sensitivity by regulating TGF-β activation in PTC. However, how this regulatory effect was achieved remained elusive.

Bernards and co-workers (15, 24) published a study on MED12 and drug resistance in multiple cancers, identifying MED12, a mediator complex subunit similar to MED16, as a critical determinant of the TKI response in NSCLCs. They claimed that the drug resistance induced by MED12 loss depended on TGF-β activation, because cytosolic MED12 interacted with immature TGF-βR2 and inhibited its glycosylation, impairing signaling activation by reducing receptor expression in the cell membrane (15, 24). Inspired by their work, we proposed that MED16 might also physically bind with TGF-βR2 and hence hamper TGF-β signaling. Indeed, our co-IP results illustrated exact interactions between MED16/TGF-βR2 as well as MED16/MED12, suggesting the synergistic action of MED16 and MED12 in TGF-β signaling suppression. Moreover, MED12^{KD} PTC cells were constructed for functional study and demonstrated that MED12 loss induced similar phenotypes in MED16 knockdown cells, including cell migration, EMT, and ^{131}I resistance.

Over recent decades, the participation of EMT in cancer drug resistance has been increasingly recognized in diverse cancers, including pancreatic cancer, bladder cancer, breast cancer, and so on (25–27), whereas the mechanism underlying this link remains elusive. One widely accepted explanation is that cancer cells undergoing EMT exhibit stem cell-like features, especially excessive drug efflux regulated by multiple cell membrane transporter proteins (4). For example, the overexpression of ABC transporters leads to 10-fold higher resistance to doxorubicin in breast cancer cells (28). Notably, the TGF-β/SMAD pathway, hyperactivated in MED16^{KD} cells with RAI resistance, is also a key pathway known to facilitate EMT by promoting the expression of mesenchymal genes, such as vimentin (9, 10, 29). In our findings, the EMT that occurred in MED16 knockdown PTC cells might have also contributed to the impaired response to ^{131}I treatment.

Considering the importance of TGF-β signaling in RAI refractory PTC cells, we reasoned that TGF-β inhibitors should resensitize MED16^{KD} cells to RAI therapy. Indeed, the combination treatment with ^{131}I and LY2157299 obtained a satisfying effect in reducing tumor growth both *in vivo* and *in vitro*, providing strong support that a small molecule drug antagonizing TGF-β might be utilized in PTC patients with MED16 dysfunction to prevent cancer recurrence and metastasis.

In conclusion, our study indicated that in PTC cells, MED16 interacted with MED12 and bound to immature TGF-βR2 to block TGF-β activation. When MED16 was knocked down, TGF-β was activated, accompanied by EMT induction, NIS repression, and radioiodine resistance. Although the exact role of TGF-β in regulating drug resistance and cancer metastasis needs further investigation, to our knowledge, we have demonstrated for the first time that a TGF-β inhibitor can significantly improve radioiodine treatment efficacy in mice with MED16^{KD} tumors, which might bring hope to advanced PTC patients with MED16 mutations or even a larger scale of PTC patients exhibiting clinical RAI-refractory disease.

Experimental procedures

Cell culture

The human thyroid papillary cancer cell lines (B-CPAP and TPC-1) were obtained from the Stem Cell Bank of the Chinese Academy of Sciences. Both cancer cell lines were maintained in RPMI 1640 medium (Gibco), supplemented with 10% fetal

Figure 5. MED16 regulated TGF-β pathway activation in PTC cells. *A* and *C*, MED16^{KD} results in strong induction of TGF-βR2 protein, Smad2, and Erk1/2 phosphorylation. Western blotting analysis of B-CPAP (*A*) and TPC-1 (*C*) cells expressing pLKO.1 or shMED16 vectors. The overexpression of MED16 showed the opposite effect; GAPDH was used as a loading control. *B* and *D*, densitometric quantification of TGF-BR2 levels normalized to GAPDH levels and presented as fold change compared with control cells (pLKO.1 or vector-treated cells). Densitometric quantification of p-ERK1/2 levels normalized to ERK1/2 levels and presented as fold change compared with control cells. Densitometric quantification of p-Smad2 levels normalized to Smad2 levels and presented as fold change compared with control cells. *E*, MED16^{KD} leads to induction of a panel of TGF-β targeting genes. mRNA expression analysis by qRT-PCR ANGPTL4, TAGLN, CRY61, and CTGF in B-CPAP and TPC-1 cells expressing pLKO.1 control or shRNAs targeting MED16 is shown. All data are presented as the means ± S.D. from three independent experiments. *, $P < 0.05$; **, $P < 0.01$; ***, $P < 0.001$; ****, $P < 0.0001$ compared with the *N.C.*, No-treatment Control Group. *F* and *G*, immunofluorescence was used to analyze the intracellular location of smad2 in B-CPAP or TPC-1 cells. *Scale bar*, 50 μm. Knockdown MED16 induced a shift in smad2 from a predominantly cytoplasmic to a predominantly nuclear localization, indicating smad2 activation.

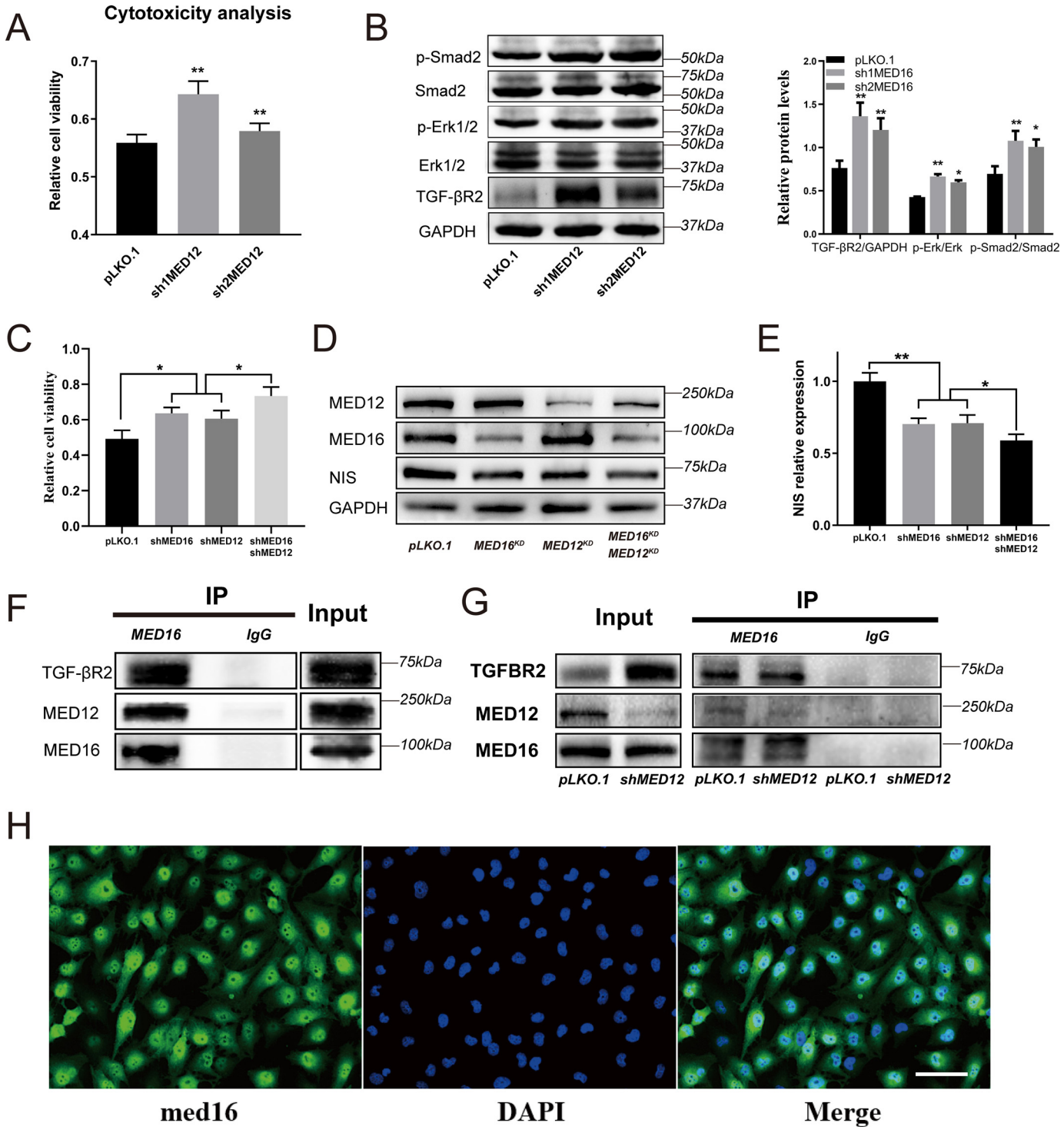

Figure 6. MED12 regulated PTC cell ^{131}I resistance and TGF-β activation. *A*, CCK8 analysis of cell viability in TPC-1 cells treated for 48 h with ^{131}I (200 μCi/well) in 96-well plates. Cell viability quantification of MED16^{KD} normalized to pLKO.1 and presented as fold change compared with untreated cells for 48 h. *B*, MED12^{KD} results in strong induction of Smad2 and Erk1/2 phosphorylation. Western blotting analysis of TPC-1 cells expressing pLKO.1 or shMED16 vectors. *C*, CCK8 analysis of cell viability in TPC-1 cells with MED12 and MED16 knockdown or with MED12/MED16 co-knockdown. *D* and *E*, the synergistic effect of MED16 and MED12 in NIS suppression. *F* and *G*, MED16 is capable of physically interacting with TGF-βR2 and MED12. Western blotting analysis of co-immunoprecipitation experiments using TPC-1 cells. *H*, immunofluorescence staining indicates extensive expression of MED16 in cytoplasm. *Scale bar*, 50 μm. *, $P <$ 0.05; **, $P < 0.01$; ***, $P < 0.001$. *DAPI*, 4′,6′-diamino-2-phenylindole.

bovine serum (FBS) and 1% penicillin/streptomycin. The cells were incubated at 37 ℃ and 5% CO_2, 95% O_2 in humidified atmosphere. HEK293T cells were used as producers of lentiviral supernatants as previous described (33).

Plasmid construction and transfection

The pLKO.1-tac was kindly provided by Dr. Xin Zhou (Sichuan University), linearized with Age1 and EcoR1, and inserted shRNA fragment. All shRNA fragments were purchased

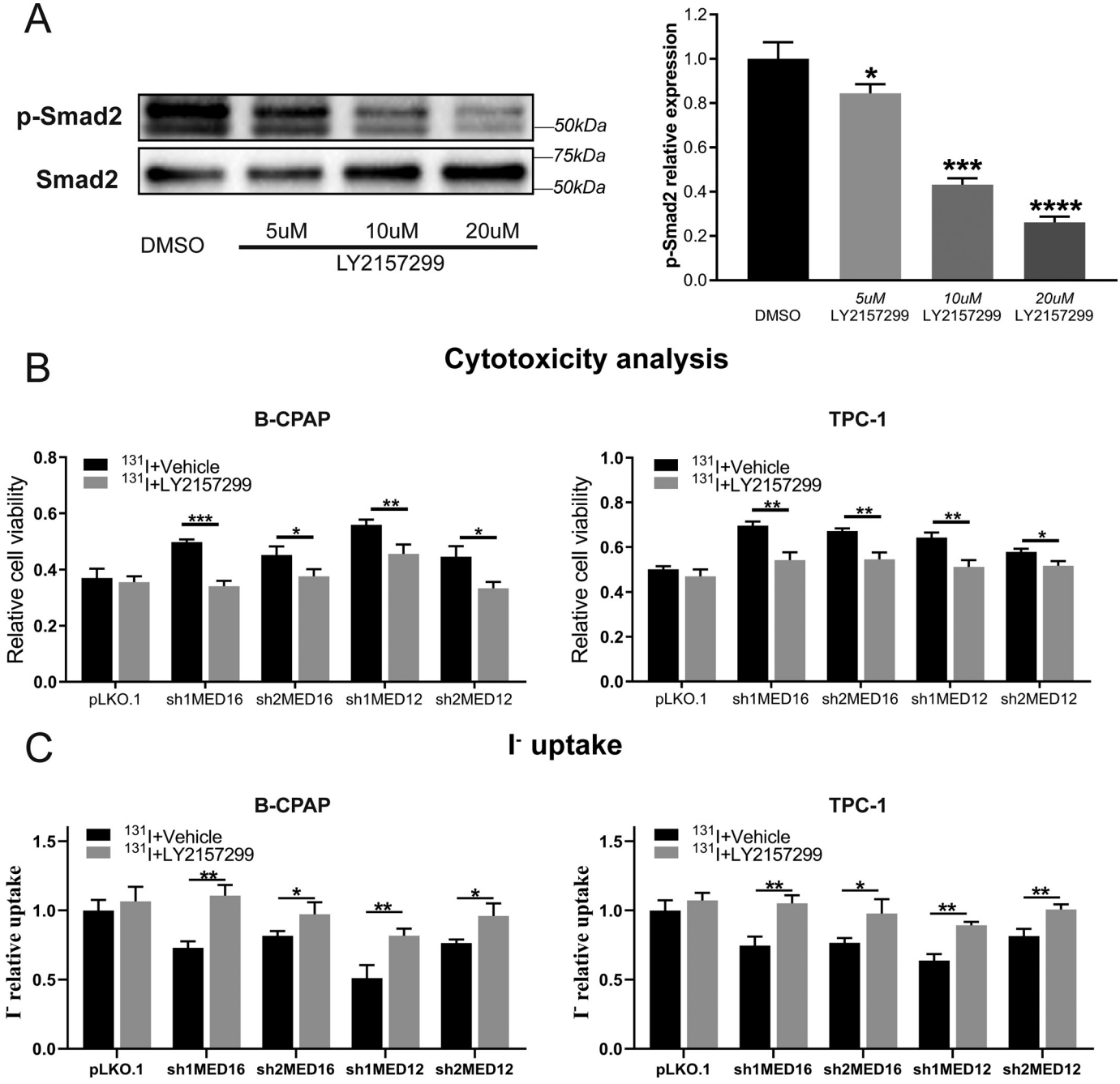

Figure 7. TGF-β inhibitor rescued the radioiodine resistance induced by MED16 and MED12 knockdown in PTC cells. *A*, Western blotting assay of Samd2 phosphorylation in B-CPAP cells in a dose-dependent manner (5–20 μM) after a 48-h incubation with LY2157299. *B*, MED16^{KD} and MED12^{KD} PTC cells were treated with ^{131}I in the presence or absence of LY2157299 at 5 μM, and then RAI cytotoxicity was analyzed by CCK8. *C*, I^- uptake analysis of MED16^{KD} and MED12^{KD} PTC cells in the presence or absence of LY2157299 at 5 μM. *, $P < 0.05$; **, $P < 0.01$; ***, $P < 0.005$; ****, $P < 0.001$.

from Tsingke Biological Technology Co., Ltd. Further details on nucleic acids and shRNA are provided in Table S3. MED16 CDS fragment was directly cloned into a lentiviral vector, pLVX-IRES-Bsd, which was derived from pLVX-IRES-ZsGreen1 (Clontech) by replacing ZsGreen1 coding sequence with that of the blasticidin resistance gene. Plasmid DNA transfections were performed with Lipofectamine 3000 (Thermo Fisher Scientific) following standard protocols in accordance with the manufacturer's guidelines.

Wound-healing assay, Transwell migration assay, and CCK-8 assay

For the wound-healing experiment, the wounds were scratched with 20-μl pipette tips in the confluent monolayers of TPC-1 and B-CPAP cells. The cells were subsequently washed with PBS twice and incubated in RPMI 1640 medium for 24 h, after which the migrating areas were assessed for analysis. For Transwell assay, the inserts with 8-μm pore membrane filters were used according to the

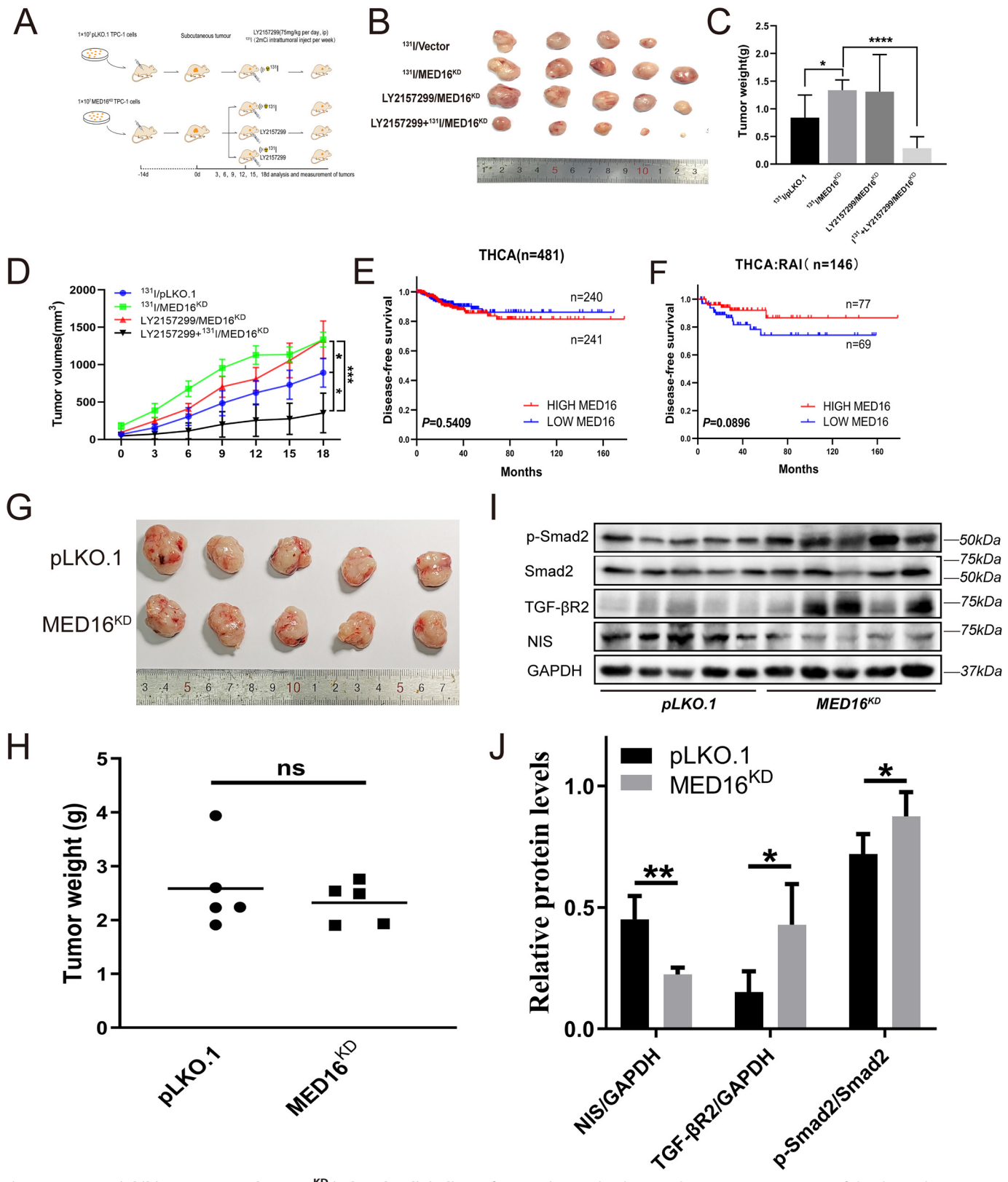

Figure 8. TGF-β inhibitor attenuated MED16^{KD} induced radioiodine refractory in PTC *in vivo*. *A*, schematic representation of the drug administration schedule for xenograft tumor model. The tumor-bearing mice receiving ^{131}I (2 mCi in 100 μl, intertumoral injection) or LY2157299 (75 mg/kg, i.p.) or the vehicle control (2% DMSO). *B*, *C*, and *D*, volumes and weight analysis of primary mice tumor in differently treated groups. *E* and *F*, disease-free survival analysis of PTC patients with differential MED16 expression. Disease-free survival for THCA with high (Q3Q4; >12.71) *versus* low (Q1Q2; <12.71) MED16 expression for the entire PTC cohort (n = 481) (*E*), RAI-treated patients (n = 146) (*F*). *G* and *H*, tumor weight of 1 × 10^7 pLKO.1 cells and MED16^{KD} cells of TPC-1 in nude mice. The number of mice in each group was 5. *I* and *J*, Western blotting assay of TGF-βR2, NIS, and p-Samd2 expression in both pLKO.1 and MED16^{KD} groups. *, P < 0.05; **, P < 0.01; ***, P < 0.005. *ns*, not significant.

manufacturer's protocol. Briefly, the suspension of 1.2×10^4cells in RPMI 1640 medium without FBS was loaded into the upper chamber of each Transwell, and 600 μl of the growth medium containing 10% FBS was added into the lower chamber acting as a chemoattractant. After a 48-h incubation, the nonmigrating cells were removed from the upper surface of the membrane; then the cells on the lower surface were fixed using 100% ethanol and stained with a 0.05% crystal violet solution, followed by gently washing with distilled water three times. The inserts were then dried in the air, and the membranes were photographed under an inverted microscope. CCK-8 assay was performed using a EnoGeneCell^{TM} counting kit 8 (CCK-8) (EnoGene, Nanjing, China) according to the manufacturer's instructions, and the absorbance was measured at 450 nm using the VICTOR $\times$ 4 multilabel plate reader.

I^- uptake assay

The cells were seeded in 6-well plates, washed with warmed Hanks' balanced salt solution (HBSS), and incubated for 30 min at 37 ℃ with 500 μl of warmed HBSS containing 0.1 μCi of ^{131}I and 10 μM nonradioactive NaI. The cells were then washed twice with cold HBSS and lysed for 5 min in 1% SDS. The cell lysates were collected for radioactivity measurement using a γ counter (Canberra-Packard, Meriden, CT, USA). Radioactivity was normalized to the amount of total protein at the time of the assay. All experiments were performed in triplicate.

Real-time PCR

First-strand cDNA was synthesized by reverse transcription reaction using oligo(dT) primers from 1 μg of total cellular RNA (Thermo Fisher Scientific). Real-time PCR was carried out with Power SYBR Green PCR Master Mix (Bio-Rad) under the following conditions: initial activation at 95 ℃ for 5 min, followed by 40 cycles of 95 ℃ for 15 s and 60 ℃ for 1 min. The primers used for real-time PCR are given in Table S3.

Animals experiment and tissue samples

Female athymic mice aged 4–6 weeks old were purchased from GemPharmatech Co., Ltd. Tumor xenografts were established by subcutaneous inoculation of 1×10^7 TPC-1 cells stably expressing shMED16 (fifteen mice) or pLKO.1 vector (five mice) into the right armpit region of nude mice. From day 3 postinjection, tumor size was measured every 3 days, and tumor volumes were calculated by the following formula: length $\times$ width$^2 \times 0.5$. The animals were assigned into four experimental groups when the volume of each tumor reached ~100 mm^3 within 3 weeks: 1) the normal tumor-bearing mice with ^{131}I treatment (2 mCi in 100 μl, intratumorally injection); 2) the MED16^{KD} tumor-bearing mice with ^{131}I treatment; 3) the MED16^{KD} tumor-bearing mice with LY2157299 treatment (75 mg/kg, intraperitoneally); and 4) the MED16^{KD} tumor-bearing mice with both ^{131}I and LY2157299 treatment. Statistical comparison of tumor growth between different groups was conducted by trend analysis. The mice were sacrificed after 18 days to collect the tumor tissue for further detection. All experimental procedures involving animals were conducted in accordance with institution guidelines and were approved by the Institutional Animal Care and Use Committee of Sichuan University.

All human PTC samples were obtained with consent as outlined by institutional review board at Sichuan University. All human studies abide by the Declaration of Helsinki principles. The MED16 transcript expression was determined using qRT-PCR.

Protein extraction and Western blotting

The cells were lysed using radioimmunoprecipitation assay buffer (Sigma–Aldrich), and total protein concentration was quantified using a BCA protein assay kit (Pierce). 20 μg of denatured protein lysate was electrophoresed using SDS-PAGE (Life Technologies). Separated proteins were transferred to nitrocellulose membranes followed by blocking in TBS with 0.1% Tween 20 (TBST) containing 5% skim milk. The blots were probed with specific antibodies (Table S4). The Western Bright Quantum detection kit (Advansta, San Jose, CA, USA) was used to visualize the detected proteins by a LAS4000 digital imaging system (Fujifilm, Tokyo, Japan), and proteins were quantified using MultiGauge software (version 3.0, Fujifilm).

Immunofluorescence

Cells were grown on glass coverslips, washed three times with PBS, fixed in 2% paraformaldehyde in PBS for 20 min at room temperature, and permeabilized with 0.2% (v/v) Triton X-100 in PBS containing 0.5% (w/v) bovine serum albumin (Sigma), Coverslips were incubated with primary Abs diluted in 0.5% bovine serum albumin for overnight at 4 ℃, washed three with PBS, and incubated with fluorescein-conjugated Abs diluted in PBS for 1 h at room temperature. After washing with PBS, the coverslips were imaged using a Zeiss fluorescence microscope.

Gene expression data analysis

Normalized gene expression data and clinical information for papillary thyroid cancer were downloaded from TCGA via cBioPortal (30, 31), whereas normalized gene expression data of normal thyroid tissue were downloaded from GTEx (32). In total, RNA-sequencing data for 510 papillary thyroid cancer samples and 653 normal thyroid samples were analyzed.

Statistics

All data are expressed as the means ± S.D. Statistical significance was determined by unpaired Student's t test. A value of $p < 0.05$ was considered statistically significant.

Data availability

All data are contained within the article.

Author contributions—H. G. and X. L. software; H. G., P. B., M. S., W. H., and F. Y. formal analysis; H. G. investigation; H. G., L. X., Q. Y., Y. L., and Y. J. methodology; H. G. writing-original draft; P. B. and M. S. data curation; L. X. and X. Z. validation; L. X., F. Y., and H. B. project administration; Q. Y. writing-review and editing; W. H. and H. B. supervision; X. Z. visualization; T. W. and Y. J. resources; F. Y. and H. B. funding acquisition.

Funding and additional information—This work was supported by Grant 81972498 from the National Natural Science Foundation of China; Grant ZYGD18012 and 2020HXFH009 from the 1.3.5 Project for Disciplines of Excellence, West China Hospital, Sichuan University; Grant 2019YFS0324 from the Research Supporting Project from Science and Technology Department of Sichuan Province; and Grant 2018-YF05-01177-SN from the Chengdu Science and Technology Bureau.

Conflict of interest—No conflict of interest exists in the submission of this manuscript from all authors.

Abbreviations—The abbreviations used are: MED16, mediator complex subunit 16; PTC, papillary thyroid cancer; NIV, sodium/iodide symporter; RAI, radioactive iodine; EMT, epithelial–mesenchymal transition; TGF, transforming growth factor; IP, immunoprecipitation; GTEx, Genotype-Tissue Expression; TCGA, The Cancer Genome Atlas; qRT-PCR, quantitative RT-PCR; qPCR, quantitative PCR; MAPK, mitogen-activated protein kinase; ERK, extracellular signal-regulated kinase; FBS, fetal bovine serum; shRNA, short hairpin RNA; HBSS, Hanks' balanced salt solution; GAPDH, glyceraldehyde-3-phosphate dehydrogenase; THCA, Thyroid carcinoma.

References

1. Torre, L. A., Bray, F., Siegel, R. L., Ferlay, J., Lortet-Tieulent, J., and Jemal, A. (2015) Global cancer statistics, 2012. *CA Cancer J. Clin.* **65,** 87–108 CrossRef Medline
2. Zhu, X., Yao, J., and Tian, W. (2015) Microarray technology to investigate genes associated with papillary thyroid carcinoma. *Mol. Med. Rep.* **11,** 3729–3733 CrossRef Medline
3. Wartofsky, L. (2010) Increasing world incidence of thyroid cancer: increased detection or higher radiation exposure? *Hormones (Athens)* **9,** 103–108 CrossRef Medline
4. American Thyroid Association (ATA) Guidelines Taskforce on Thyroid Nodules and Differentiated Thyroid Cancer, Cooper, D. S., Doherty, G. M., Haugen, B. R., Hauger, B. R., Kloos, R. T., Lee, S. L., Mandel, S. J., Mazzaferri, E. L., McIver, B., Pacini, F., Schlumberger, M., Sherman, S. I., Steward, D. L., and Tuttle, R. M. (2009) Revised American Thyroid Association management guidelines for patients with thyroid nodules and differentiated thyroid cancer. *Thyroid* **19,** 1167–1214 CrossRef Medline
5. Shoup, M., Stojadinovic, A., Nissan, A., Ghossein, R. A., Freedman, S., Brennan, M. F., Shah, J. P., and Shaha, A. R. (2003) Prognostic indicators of outcomes in patients with distant metastases from differentiated thyroid carcinoma. *J. Am. Coll. Surg.* **197,** 191–197 CrossRef Medline
6. Durante, C., Haddy, N., Baudin, E., Leboulleux, S., Hartl, D., Travagli, J. P., Caillou, B., Ricard, M., Lumbroso, J. D., De Vathaire, F., and Schlumberger, M. (2006) Long-term outcome of 444 patients with distant metastases from papillary and follicular thyroid carcinoma: benefits and limits of radioiodine therapy. *J. Clin. Endocrinol. Metab.* **91,** 2892–2899 CrossRef Medline
7. Grubeck-Loebenstein, B., Buchan, G., Sadeghi, R., Kissonerghis, M., Londei, M., Turner, M., Pirich, K., Roka, R., Niederle, B., and Kassal, H. (1989) Transforming growth factor β regulates thyroid growth: role in the pathogenesis of nontoxic goiter. *J. Clin. Invest.* **83,** 764–770 CrossRef Medline
8. Franzén, A., Piek, E., Westermark, B., ten Dijke, P., and Heldin, N. E. (1999) Expression of transforming growth factor-β1, activin A, and their receptors in thyroid follicle cells: negative regulation of thyrocyte growth and function. *Endocrinology* **140,** 4300–4310 CrossRef Medline
9. Bravo, S. B., Pampín, S., Cameselle-Teijeiro, J., Carneiro, C., Domínguez, F., Barreiro, F., and Alvarez, C. V. (2003) TGF-β–induced apoptosis in human thyrocytes is mediated by p27kip1 reduction and is overridden in neoplastic thyrocytes by NF-κB activation. *Oncogene* **22,** 7819–7830 CrossRef Medline
10. Lamouille, S., Connolly, E., Smyth, J. W., Akhurst, R. J., and Derynck, R. (2012) TGF-β–induced activation of mTOR complex 2 drives epithelial–mesenchymal transition and cell invasion. *J. Cell Sci.* **125,** 1259–1273 CrossRef Medline
11. Riesco-Eizaguirre, G., Rodríguez, I., De la Vieja, A., Costamagna, E., Carrasco, N., Nistal, M., and Santisteban, P. (2009) The BRAFV600E oncogene induces transforming growth factor β secretion leading to sodium iodide symporter repression and increased malignancy in thyroid cancer. *Cancer Res.* **69,** 8317–8325 CrossRef Medline
12. Ma, S., Wang, Q., Ma, X., Wu, L., Guo, F., Ji, H., Liu, F., Zhao, Y., and Qin, G. (2016) FoxP3 in papillary thyroid carcinoma induces NIS repression through activation of the TGF-β1/Smad signaling pathway. *Tumour Biol.* **37,** 989–998 CrossRef Medline
13. Syring, I., Klümper, N., Offermann, A., Braun, M., Deng, M., Boehm, D., Queisser, A., von Mässenhausen, A., Brägelmann, J., Vogel, W., Schmidt, D., Majores, M., Schindler, A., Kristiansen, G., Müller, S. C., *et al.* (2016) Comprehensive analysis of the transcriptional profile of the mediator complex across human cancer types. *Oncotarget* **7,** 23043–23055 CrossRef Medline
14. Schiano, C., Casamassimi, A., Rienzo, M., de Nigris, F., Sommese, L., and Napoli, C. (2014) Involvement of mediator complex in malignancy. *Biochim. Biophys. Acta* **1845,** 66–83 CrossRef Medline
15. Huang, S., Hölzel, M., Knijnenburg, T., Schlicker, A., Roepman, P., McDermott, U., Garnett, M., Grernrum, W., Sun, C., Prahallad, A., Groenendijk, F. H., Mittempergher, L., Nijkamp, W., Neefjes, J., Salazar, R., *et al.* (2012) MED12 controls the response to multiple cancer drugs through regulation of TGF-β receptor signaling. *Cell* **151,** 937–950 CrossRef Medline
16. Cancer Genome Atlas Research Network (2014) Integrated genomic characterization of papillary thyroid carcinoma. *Cell* **159,** 676–690 CrossRef Medline
17. Ferlay, J., Colombet, M., Soerjomataram, I., Mathers, C., Parkin, D. M., Piñeros, M., Znaor, A., and Bray, F. (2019) Estimating the global cancer incidence and mortality in 2018: GLOBOCAN sources and methods. *Int. J. Cancer* **144,** 1941–1953 CrossRef Medline
18. Nixon, I. J., Whitcher, M. M., Palmer, F. L., Tuttle, R. M., Shaha, A. R., Shah, J. P., Patel, S. G., and Ganly, I. (2012) The impact of distant metastases at presentation on prognosis in patients with differentiated carcinoma of the thyroid gland. *Thyroid* **22,** 884–889 CrossRef Medline
19. Dohán, O., De la Vieja, A., Paroder, V., Riedel, C., Artani, M., Reed, M., Ginter, C. S., and Carrasco, N. (2003) The sodium/iodide symporter (NIS): characterization, regulation, and medical significance. *Endocr. Rev.* **24,** 48–77 CrossRef Medline
20. Liu, J., Liu, Y., Lin, Y., and Liang, J. (2019) Radioactive iodine-refractory differentiated thyroid cancer and redifferentiation therapy. *Endocrinol. Metab. (Seoul)* **34,** 215–225 CrossRef Medline
21. Xing, M., Westra, W. H., Tufano, R. P., Cohen, Y., Rosenbaum, E., Rhoden, K. J., Carson, K. A., Vasko, V., Larin, A., Tallini, G., Tolaney, S., Holt, E. H., Hui, P., Umbricht, C. B., Basaria, S., *et al.* (2005) BRAF mutation predicts a poorer clinical prognosis for papillary thyroid cancer. *J. Clin. Endocrinol. Metab.* **90,** 6373–6379 CrossRef Medline
22. Ricarte-Filho, J. C., Ryder, M., Chitale, D. A., Rivera, M., Heguy, A., Ladanyi, M., Janakiraman, M., Solit, D., Knauf, J. A., Tuttle, R. M., Ghossein, R. A., and Fagin, J. A. (2009) Mutational profile of advanced primary and metastatic radioactive iodine-refractory thyroid cancers reveals distinct pathogenetic roles for BRAF, PIK3CA, and AKT1. *Cancer Res.* **69,** 4885–4893 CrossRef Medline
23. Costamagna, E., García, B., and Santisteban, P. (2004) The functional interaction between the paired domain transcription factor Pax8 and Smad3 is involved in transforming growth factor-β repression of the sodium/iodide symporter gene. *J. Biol. Chem.* **279,** 3439–3446 CrossRef Medline
24. Brunen, D., Willems, S. M., Kellner, U., Midgley, R., Simon, I., and Bernards, R. (2013) TGF-β: an emerging player in drug resistance. *Cell Cycle* **12,** 2960–2968 CrossRef Medline
25. Arumugam, T., Ramachandran, V., Fournier, K. F., Wang, H., Marquis, L., Abbruzzese, J. L., Gallick, G. E., Logsdon, C. D., McConkey, D. J., and

Choi, W. (2009) Epithelial to mesenchymal transition contributes to drug resistance in pancreatic cancer. *Cancer Res.* **69,** 5820–5828 CrossRef Medline
26. Mittal, V. (2018) Epithelial mesenchymal transition in tumor metastasis. *Annu. Rev. Pathol.* **13,** 395–412 CrossRef Medline
27. McConkey, D. J., Choi, W., Marquis, L., Martin, F., Williams, M. B., Shah, J., Svatek, R., Das, A., Adam, L., Kamat, A., Siefker-Radtke, A., and Dinney, C. (2009) Role of epithelial-to-mesenchymal transition (EMT) in drug sensitivity and metastasis in bladder cancer. *Cancer Metastasis Rev.* **28,** 335–344 CrossRef Medline
28. Saxena, M., Stephens, M. A., Pathak, H., and Rangarajan, A. (2011) Transcription factors that mediate epithelial–mesenchymal transition lead to multidrug resistance by upregulating ABC transporters. *Cell Death Dis.* **2,** e179 CrossRef Medline
29. Zhao, L., Liu, S., Che, X., Hou, K., Ma, Y., Li, C., Wen, T., Fan, Y., Hu, X., Liu, Y., and Qu, X. (2015) Bufalin inhibits TGF-β–induced epithelial-to-mesenchymal transition and migration in human lung cancer A549 cells by downregulating TGF-β receptors. *Int. J. Mol. Med.* **36,** 645–652 CrossRef Medline
30. Cerami, E., Gao, J., Dogrusoz, U., Gross, B. E., Sumer, S. O., Aksoy, B. A., Jacobsen, A., Byrne, C. J., Heuer, M. L., Larsson, E., Antipin, Y., Reva, B., Goldberg, A. P., Sander, C., and Schultz, N. (2012) The cBio cancer genomics portal: an open platform for exploring multidimensional cancer genomics data. *Cancer Discov.* **2,** 401–404 CrossRef Medline
31. Gao, J., Aksoy, B. A., Dogrusoz, U., Dresdner, G., Gross, B., Sumer, S. O., Sun, Y., Jacobsen, A., Sinha, R., Larsson, E., Cerami, E., Sander, C., and Schultz, N. (2013) Integrative analysis of complex cancer genomics and clinical profiles using the cBioPortal. *Sci. Signal.* **6,** pl1 CrossRef Medline
32. GTEx Consortium (2013) The Genotype-Tissue Expression (GTEx) project. *Nat. Genet.* **45,** 580–585 CrossRef Medline
33. Ochiai, H., Takenobu, H., Nakagawa, A., Yamaguchi, Y., Kimura, M., Ohira, M., Okimoto, Y., Fujimura, Y., Koseki, H., Kohno, Y., Nakagawara, A., and Kamijo, T. (2010) Bmi1 is a MYCN target gene that regulates tumorigenesis through repression of KIF1Bbeta and TSLC1 in neuroblastoma. *Oncogene.* **29,** 2681–2690 CrossRef Medline